JGR Earth Surface

RESEARCH ARTICLE
10.1029/2023JF007154

Tree-Ring Derived Avalanche Frequency and Climate Associations in a High-Latitude, Maritime Climate

E. H. Peitzsch[1], E. Hood[2], J. R. Harley[2], D. K. Stahle[1], N. E. Kichas[3], and G. J. Wolken[4,5]

[1]U.S. Geological Survey, Northern Rocky Mountain Science Center, West Glacier, MT, USA, [2]Program on the Environment and Alaska Coastal Rainforest Center, University of Alaska Southeast, Juneau, AK, USA, [3]Montana State University, Bozeman, MT, USA, [4]Alaska Division of Geological & Geophysical Surveys, Fairbanks, AK, USA, [5]International Arctic Research Center, University of Alaska Fairbanks, Fairbanks, AK, USA

Abstract Snow avalanches are a natural hazard in mountainous areas worldwide with severe impacts that include fatalities, damage to infrastructure, disruption to commerce, and landscape disturbance. Understanding long-term avalanche frequency patterns, and associated climate and weather influences, improves our understanding of how climate change may affect avalanche activity. We used dendrochronological techniques to evaluate the historical frequency of large magnitude avalanches (LMAs) in the high-latitude climate of southeast Alaska, United States. We collected 434 cross sections throughout six avalanche paths near Juneau, Alaska. This resulted in 2706 identified avalanche growth disturbances between 1720 and 2018, which allowed us to reconstruct 82 years with LMA activity across three sub-regions. By combining this tree-ring-derived avalanche data set with a suite of climate and atmospheric variables and applying a generalized linear model to fit a binomial regression, we found that February and March precipitation and the Oceanic Niño Index (ONI) were significant predictors of LMA activity in the study area. Specifically, LMA activity occurred during winters with substantial February and March precipitation and neutral or negative (cold) ONI values, while years not characterized by LMAs occur more frequently during warm winters (positive ONI values). Our examination of the climate-avalanche relationship in southeast Alaska sheds light on important climate variables and physical processes associated with LMA years. These results can be used to inform long-term infrastructure planning and avalanche mitigation operations in an urban area, such as Juneau, where critical infrastructure is subject to substantial avalanche hazard.

Plain Language Summary Snow avalanches pose a hazard in mountainous regions throughout the world. By calculating how often large destructive avalanches recur in an area and combining these avalanche records with climate data from the same period, we gain a better understanding of how climate influences avalanche activity. To achieve this, we collected samples from trees in avalanche paths and analyzed tree growth rings to determine how often an avalanche occurs in a single avalanche path. We were able to date large avalanches from tree-ring records because an avalanche can cause mechanical damage to a tree and result in a growth disturbance for that year. We completed this analysis across six avalanche paths in southeast Alaska, United States. We found that large avalanches tended to occur during winters with higher-than-normal mid-winter precipitation and those with a neutral or negative (i.e., cold) Oceanic Niño Index, an index representative of short-term temperature variability in the study area. Our results suggest that temperature influences the type of precipitation (rain vs. snow) and, when combined with mid-winter precipitation, influences whether a winter is characterized by large avalanches or not. These results can be used to inform infrastructure planning and avalanche mitigation in and around Juneau, Alaska.

Key Points:

- We collected 434 cross sections throughout six avalanche paths, resulting in 2706 identified growth disturbances due to avalanches
- Large magnitude avalanches (LMAs) in the study area occur every 9 years (median)
- Mid-winter precipitation amount and type, as driven by temperature, influence the frequency of LMAs in this high latitude maritime climate

Supporting Information:

Supporting Information may be found in the online version of this article.

Correspondence to:

E. H. Peitzsch,
epeitzsch@usgs.gov

Citation:

Peitzsch, E. H., Hood, E., Harley, J. R., Stahle, D. K., Kichas, N. E., & Wolken, G. J. (2023). Tree-ring derived avalanche frequency and climate associations in a high-latitude, maritime climate. *Journal of Geophysical Research: Earth Surface*, *128*, e2023JF007154. https://doi.org/10.1029/2023JF007154

Received 7 MAR 2023
Accepted 25 JUL 2023

Author Contributions:

Conceptualization: E. H. Peitzsch, E. Hood
Data curation: E. Hood, D. K. Stahle, N. E. Kichas, G. J. Wolken
Formal analysis: E. H. Peitzsch, J. R. Harley, D. K. Stahle, N. E. Kichas
Funding acquisition: E. H. Peitzsch, E. Hood, G. J. Wolken
Methodology: E. H. Peitzsch, D. K. Stahle, G. J. Wolken
Project Administration: E. H. Peitzsch, E. Hood
Supervision: E. H. Peitzsch, E. Hood
Visualization: E. H. Peitzsch, J. R. Harley
Writing – original draft: E. H. Peitzsch, E. Hood, J. R. Harley

1. Introduction

Snow avalanches affect transportation corridors and settlements throughout the world. Understanding long-term avalanche frequency patterns, and associated climate and weather influences, furthers our understanding of how climate change may affect avalanche activity and associated societal impacts. Avalanches also play an important ecological role by modifying landscape and habitat characteristics (Bebi et al., 2009; Rixen et al., 2007). Climate (e.g., coastal, continental) serves as a background influence on snowpack characteristics that drive long-term patterns in avalanche activity (Armstrong & Armstrong, 1987; Mock & Birkeland, 2000; Mock et al., 2016) or prevalent avalanche problem type (Haegeli et al., 2021), while weather directly influences snowpack structure and avalanches on daily to seasonal timescales. In addition, variability in synoptic-scale

Writing – review & editing: E. H. Peitzsch, E. Hood, J. R. Harley, D. K. Stahle, N. E. Kichas, G. J. Wolken

atmospheric circulation and persistent climate modes (i.e., ocean-atmosphere teleconnections such as the El Niño Southern Oscillation, ENSO and the Pacific Decadal Oscillation, PDO) can have substantial effects on snowpack processes (Abatzoglou, 2010; McCabe, 1994; McCabe & Dettinger, 2002; Mock, 1996; Pederson et al., 2011a, 2011b, 2013) as well as avalanche frequency and behavior (Birkeland & Mock, 1996; Birkeland et al., 2001; Fitzharris & Bakkehoi, 1986; Fitzharris & Schaerer, 1980; Peitzsch, Pederson, et al., 2021).

Recent studies examined the effects of climate change and increasing winter air temperature on avalanche frequency, magnitude, and trends. For instance, in North America, Peitzsch, Pederson, et al. (2021) showed a decrease in the probability of large magnitude avalanche (LMA) years in the northern Rocky Mountains, United States, due primarily to temperature-driven snowpack decline, but also suggested that increased spring precipitation buffered this decreasing trend. Similarly, in Glacier National Park, British Columbia, Canada, Bellaire et al. (2016) found several significant trends between 1965 and 2014 for weather and snowpack variables consistent with a warming climate, such as warmer temperatures and less snowfall over monthly and seasonal scales.

Across the European Alps, studies on climate change effects on snow avalanches have come to differing conclusions depending on the region. For example, in the Swiss Alps, Laternser and Schneebeli (2003) found a gradually increasing mean snow depth, persistence of continuous snow cover, and number of snowfall days to increase until the 1980s, after which a significant decrease in each variable occurred. Though snow conditions had changed over a 50-year period, an associated long-term change in avalanche activity was not discernible (Laternser & Schneebeli, 2002). More recently, in the Vosges Mountains, France, Giacona et al. (2021) found that winter warming led to a decrease in the number of avalanches and a reduction in avalanche runout extent at lower elevations. Similarly, in the French Alps, Eckert et al. (2013) found a general decrease in dry snow avalanches since the mid-1970s as well as an increase in runout altitude (i.e., a decreased runout distance) of infrequent LMAs from 1980 to 2000, suggesting a potential change in avalanche character from dry snow to wet snow avalanches. On the other hand, Eckert et al. (2009) found no discernible change in overall avalanche occurrence processes that could be associated with climate change over the past 60 years in the northern French Alps, while Pielmeier et al. (2013) found an increase in the proportion of wet snow avalanches in the Swiss Alps from 1952 to 2013. In the western Himalaya, Ballesteros-Canovas et al. (2018) reported an increase in the probability of wet snow avalanches in the late 20th century.

Several studies in North America investigating the relationship between long-term avalanche frequency patterns and large-scale climate patterns and teleconnections reveal a complex interaction that is often difficult to disentangle from short-term synoptic weather events. For instance, Mock and Birkeland (2000) investigated atmospheric circulation and avalanche climate associations in the western United States and found the Pacific-North American teleconnections (both phases) to be correlated with several avalanche-climate patterns. Fitzharris and Schaerer (1980) found associations between major avalanche winters at Rogers Pass, British Columbia, Canada, with either strong zonal flow that brought heavy snow and rising temperatures or periods of sustained meridional flow resulting in extended cold and below average snowfall followed by wet storm systems from the Pacific. Peitzsch, Pederson, et al. (2021) found winters with persistent low pressure, negative anomalies of the PDO and positive snow depth anomalies as a major contributor to years with LMA activity.

Studies examining climate-avalanche relationships require long-term avalanche and climate data. However, in the western United States, complete long-term avalanche records are sparse or non-existent. Dendrochronological studies are a common method of reconstructing avalanche chronologies and have been used in a wide variety of snow climates (Ballesteros-Canovas et al., 2018; Favillier et al., 2018; Hebertson & Jenkins, 2003; Martin & Germain, 2016; Peitzsch, Pederson, et al., 2021; Pop et al., 2018). Here, we used a tree-ring based avalanche occurrence data set in a high-latitude, maritime climate coupled with long-term climate data to examine the climate drivers of LMA frequency in southeast Alaska. Our objective was to develop a regional LMA chronology for the study area and identify the climate variables and ocean/atmospheric teleconnections associated with LMA frequency. Building upon well-established avalanche-dendrochronological techniques (Burrows & Burrows, 1976; Butler & Sawyer, 2008), and more recent advances in this field (Corona et al., 2012; Favillier et al., 2018), we strategically sampled six avalanche paths near Juneau, Alaska that are representative of the regional topography and climate. We employed a strategic regional sampling methodology that aligns the spatial and temporal scales of the avalanche process to the potential influence of synoptic atmospheric variables. For instance, in this study, we examine relationships between avalanche frequency and regional climate patterns. However, tree-ring samples are only available and collected at an avalanche path scale. Therefore, we sampled a

network of avalanche paths spaced across the core of the climatically similar region similar to Peitzsch, Hendrikx, et al. (2021) (see Section 2.2). Understanding the regional spatio-temporal nature of LMA frequency and associated climate drivers helps improve avalanche forecasting and, ultimately, our understanding of this dynamic natural hazard in a changing climate.

2. Materials and Methods

2.1. Study Area

Our study area is comprised of six individual avalanche paths in the Coast Mountains of southeastern Alaska near Juneau, which is the most populous city in the region (Figure 1). We sampled pairs of avalanche paths in three distinct subregions within the same general maritime climate type (Shandro & Haegeli, 2018), providing climatological coherence across the study region (Lader et al., 2020). Mean monthly temperatures range from −2 to 14°C and mean annual precipitation is 1,400 mm in Juneau. Winter snowfall at sea level measures 0.4 m of water equivalent (w.e.) with greater than 10 m w.e. at higher elevations on the nearby Juneau Icefield (Pelto et al., 2013). The region is part of the world's largest contiguous coastal temperate rainforest and composed primarily of spruce-hemlock forests at lower elevations with alpine tundra, bedrock, and extensive glacier coverage at upper elevations. The avalanche paths in this study extend from sea level to 1,000 m above sea level (a.s.l.) and include a variety of aspects (Table 1).

Long-term historical observational avalanche records in the region are scarce and generally limited to LMAs directly affecting the City and Borough of Juneau (Margreth, 2011) and surrounding roads and infrastructure (Wilbur et al., 2010). As such, we collected tree-ring samples in avalanche paths included in these long-term records, as well as in paths with more recent and consistent avalanche activity to allow for a qualitative comparison of avalanche events documented in the historical record versus those registered in tree-rings. A formal quantitative analysis of tree-ring-derived avalanche frequency compared to these historical records would not be reflective of the true reliability of tree-ring methods due primarily to the incomplete historical record.

2.2. Sample Collection and Processing

The use of tree-rings in avalanche studies is robust, but due to the inherent decrease in data quantity moving further back in time, this method can lead to an underestimation of avalanche activity (Corona et al., 2012). To help alleviate the issue of missing avalanche years because of successive large avalanches in any one given avalanche path and to obtain a reasonable regional estimate of avalanche frequency, we employed a regional sampling strategy using full cross-sectional samples from trees (Peitzsch, Hendrikx, et al., 2021). In this sampling method, we utilized the concept of scale triplet to synchronize the measurement scale to the process scale of avalanches. By incorporating the scale triplet concept, we are able to better understand the characteristics of the topic, the scale at which samples should be collected, and how we can estimate the measurements across space. The scale at which measurements are made can often differ from the scale necessary for predictive purposes, making inference problematic (Blöschl, 1999). As such, we considered spacing (the distance between avalanche paths), extent (the overall spatial domain of our study area), and support (the size and location of the individual trees (samples) within each avalanche path) (Blöschl, 1999). We utilized a nested design where we sampled two individual paths that were either adjacent to each other or within the same drainage to capture the sub-region and then a total of six avalanche paths across the broader region.

We define LMAs as avalanches of approximately size D3 or greater, which translates to a destructive potential that could "bury and destroy a car, damage a truck, destroy a wood frame house, or break a few trees" (Greene et al., 2016). We also used LMA observations within the past 15 years to constrain our sampling extent. Based on previous work analyzing sample sizes in avalanche-dendrochronological research (Corona et al., 2012; Germain, 2016), we sampled between 51 and 147 tree stems per avalanche path, resulting in 426 cross-section samples from 434 trees across the study area. The three species we sampled were mountain hemlock (Tsuga mertensiana; TSME), Alaska yellow-cedar (Callitropsis nootkatensis; CANO), and Sitka spruce (Picea sitchensis; PISI).We sampled cross sections in this study due to the availability of downed and standing dead trees, and, more importantly, cross sections provide a more robust and complete growth disturbance (GD) and avalanche history when compared to traditional increment cores (Peitzsch, Hendrikx, et al., 2021).

For individual tree samples, we extracted cross sections at the location of visually identified scars or just above the root buttress. For downed trees, we collected location characteristics, including the presence or absence of ground-attached roots and the distance to the location where the tree was uprooted, that were used to identify

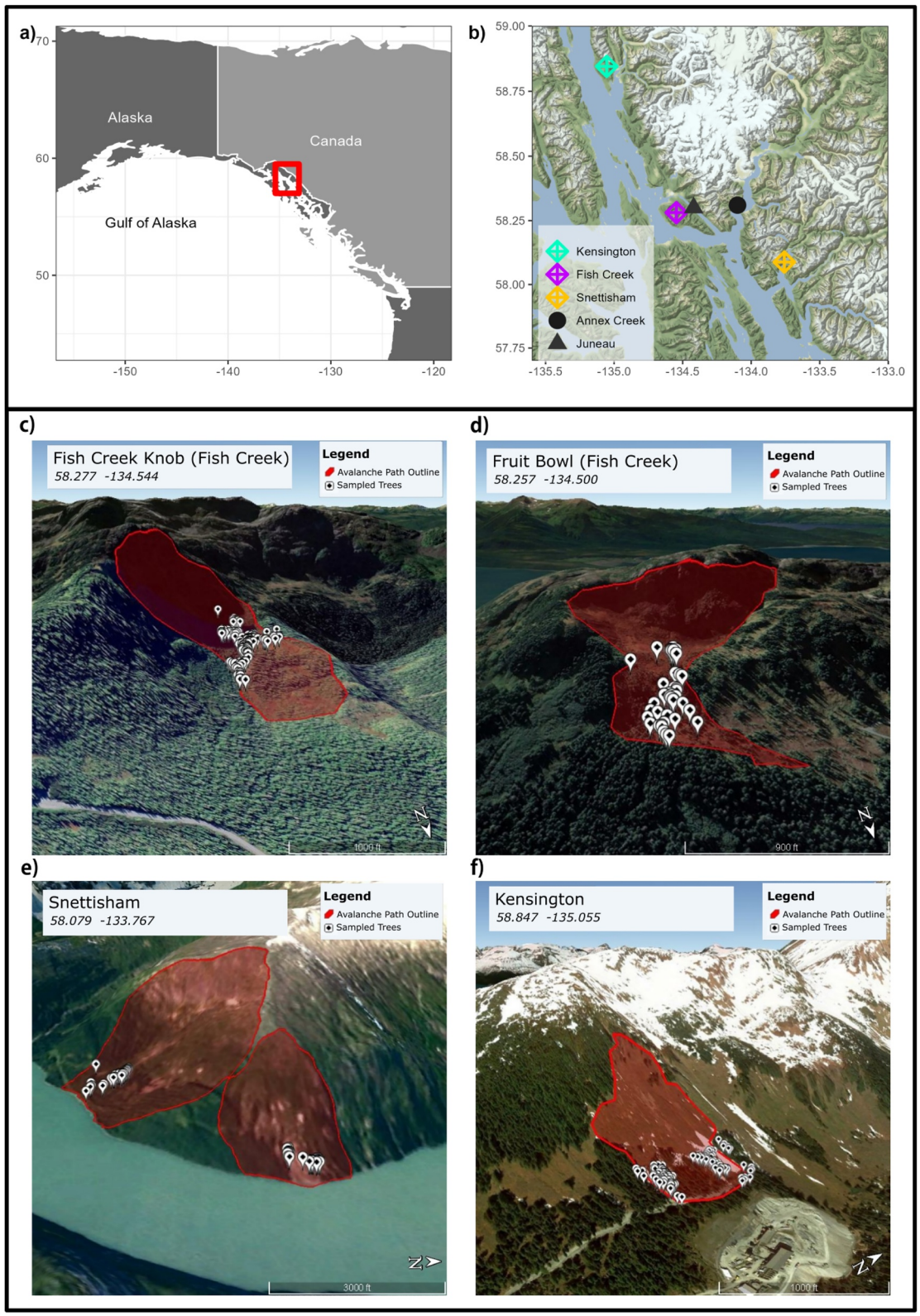

Figure 1. (a) Regional overview showing the location of the Juneau area, southeast Alaska. (b) Shaded relief map of the study region with three slide path locations identified (squares) along with the city of Juneau and the Global Historic Climate Network site of Annex Creek. (c–f) Satellite imagery showing avalanche paths including starting zones and the location of dendrochronology samples within each slide path. Note: white pins with black dots denote tree-ring sample locations. Satellite and map imagery: © Google (2023).

Table 1
Topographic Characteristics of Avalanche Paths in the Study Region of Southeast Alaska

Subregion-path	# Trees/# samples	Full path elevation (range) (m)	Starting zone slope (mean) (°)	Area (km^2)	Length (m)	Aspect (mean)
Kensington—Jualin Portal (JP)	62/63	334–505	38	0.03	230	NE
Kensington—Kensington Portal (KP)	52/56	334–616	43	0.05	360	NE
Fish Creek—Fruit Bowl (FB)	51/51	593–868	33	0.16	850	E
Fish Creek (FC)—Fish Creek Knob (FK)	147/149	416–896	38	0.37	1,070	SW
Snettisham—South Crater (SC)	62/63	0–653	35	0.55	950	E
Snettisham—4–6 Diverter (4–6)	52/52	4.5–1,000	39	1.38	1,600	SE
All Paths	426/434	0–1,000	33–43	2.54	–	–

if the tree was in place or transported from its original growth position. In addition to collecting cross sections, we extracted 5mm increment cores from living trees with obvious scarring or flagging along the avalanche path margin and in the runout zone. At every sample location where cross sections or increment cores were collected, we took a photograph annotated with the sample ID number, recorded the GPS coordinates for the sample (accuracy 1–3 m), and noted the upslope direction (when discernible) as well as the extent of scarring on sampled trees (Peitzsch et al., 2023). We also extracted increment cores from living trees in the surrounding gallery forest (i.e., trees not impacted by avalanches) for cross-dating purposes. We used nearby tree-ring records from the International Tree-Ring Databank (ITRDB, 2020) to facilitate crossdating of the sampled materials.

2.3. Avalanche Year Identification and Chronology Reconstruction

We analyzed samples for signs of traumatic impact events (hereafter "responses") likely caused by snow avalanches. We adapted a classification system from previous dendrogeomorphological studies to qualitatively rank the trauma severity and tree growth response (Nowacki & Abrams, 1997; Stoffel et al., 2010) from avalanche impacts using numerical scores ranked 1 through 5 (Table S1 in Supporting Information S1) (Peitzsch, Hendrikx, et al., 2021; Reardon et al., 2008). This classification scheme identified more prominent avalanche damage responses with higher-quality scores and allowed us to remain consistent with previous work (Corona et al., 2012; Favillier et al., 2018). We included only the highest quality response as the response for a given year in a given tree.

To generate avalanche event chronologies and estimate return periods for each path as well as for the entire study area, we utilized the package *slideRun*, an extension of the *burnR* library (Malevich et al., 2018) within the R programming environment. We calculated the age of each tree sampled and the number of responses per year in each avalanche path and computed descriptive statistics for the entire data set. Estimates of avalanche path return intervals (RIs) should be viewed as potential maximum RI values due to the successive loss of samples and decreasing sample number back through time. RIs, typically reported in years, are defined as the time period between occurrences of an avalanche event of a given or greater magnitude.

We used a multistep process to reconstruct avalanche chronologies on three different spatial scales: individual paths, three subregions, and the entire region (Favillier et al., 2017, 2018; Peitzsch, Hendrikx, et al., 2021). First, we calculated the ratio of trees exhibiting GDs over the number of samples alive in year t to provide the index I_t (Shroder, 1978):

$$I_t = \left(\frac{\sum_{i=1}^{n}(R_t)}{\sum_{i=1}^{n}(A_t)} \right) \times 100 \quad (1)$$

where R_t is the number of trees recording a GD in year t with A_t representing the number of trees alive in our samples in year t.

We then used double thresholds to estimate the minimum absolute number of GDs and a minimum percentage of samples exhibiting GDs per year (I_t) based on sample size (N) following thresholds established by Corona

et al. (2012) and Favillier et al. (2018): N = 10–20 (GD ≥ 3 and $I_t \geq 15\%$), N = 21–50 (GD ≥ 5 and $I_t \geq 10\%$), N = 51–100 (GD ≥ 7 and $I_t \geq 7\%$), and $N > 100$ (GD ≥ 9 and $I_t \geq 4.5\%$).

We used the chronologies derived from this process to calculate a weighted index factor (W_{it}). We used this established threshold approach since it has been broadly employed in the literature and allows for the comparability of our avalanche chronology to results reported in other studies. We adapted previous equations of a weighted response index (Kogelnig-Mayer et al., 2011) to our five-scale ranking quality classification to derive the W_{it}:

$$W_{it} = \frac{\left(\left(\sum_{i=1}^{n} T_{C_1} * 7\right) + \left(\sum_{i=1}^{n} T_{C_2} * 5\right) + \left(\sum_{i=1}^{n} T_{C_3} * 3\right) + \left(\sum_{i=1}^{n} T_{C_4,C_5}\right)\right)}{\sum_{i=1}^{n} A_t} \quad (2)$$

where the sum of trees with scars or injuries (C1–C5) was multiplied by a factor of 7, 5, 3, 1, and 1, respectively.

Next, we classified W_{it} into high, medium, and low confidence events using the thresholds detailed in Favillier et al. (2018), in which high is $W_{it} \geq 0.3$, medium is $0.3 > W_{it} \geq 0.2$, and low is $W_{it} < 0.2$. This provided another step for discriminating the avalanche response from noise. We included all events with medium to high confidence in the next analysis. We then estimated the number of avalanche years, descriptive statistics for RIs, and the annual probability (1/RI) for each path, subregion, and region. We used these RI values, which were determined after filtering events throughout the study. Finally, we compared RIs between individual paths and across subregions using analysis of variance and Tukey's Honest Significance Difference test (Ott & Longnecker, 2016).

We completed this multi-step process for each individual path and then grouped each path within each sub-region together and completed the same process rather than simply aggregating the avalanche years together for each path and classifying those years as avalanche years for the sub-region. This method attempts to limit the potential bias of any one avalanche path within a sub-region (Favillier et al., 2023; Peitzsch, Hendrikx, et al., 2021) but can also reveal a regional avalanche year when two or more paths combined meet the existing thresholds.

2.4. Climate and Weather Data

For our generalized linear model (glm) (described in Section 2.5), we used climate data from Annex Creek (28 m a.s.l., Global Historic Climate Network (GHCN) ID: USC00500363), which has a record extending back to 1917 (Table 2). We chose the Annex Creek station because of the length of record and because it is located to the east of Juneau (Figure 1), and it has a colder and wetter climate than the other local, long-term climate station at the Juneau airport (5 m a.s.l., GHCN ID: USW00025309, 1933–2020 climate record). As a result, Annex Creek is more representative of the weather in the higher elevation starting zones of the coastal avalanche paths we sampled. We also compared Annex Creek temperature and precipitation records to local stations at Snettisham and Kensington that have more temporally limited data sets to assess regional climate coherence (Figure S1 in Supporting Information S1).

The Annex Creek climate data set extends from 1917 to 2020, and we used the following climate parameters in our analyses: daily mean, maximum, and minimum temperature (°C); precipitation (mm), snow depth (mm), and snowfall (mm). We used climate data from the Juneau Airport to impute missing observations from the Annex Creek data set as the Annex Creek record had periods of missing data, primarily in the 1990s. However, climate data from these sites are highly correlated (Figure 2). We compared observed values for each variable for the Juneau Airport to the long-term daily mean for that particular date, and the magnitude of change (e.g., 20% above normal) was then multiplied to the daily average value for Annex Creek on that date to create an imputed value for each climate parameter. Overall, between 16% and 27% of the Annex Creek data record for the climate parameters we used was imputed using data from the Juneau Airport. This is slightly more than the typical threshold of 10% of missing data, but the climatic coherence across this region (Figure S1 in Supporting Information S1) suggests using the longer-term Juneau Airport record to complete the more representative Annex Creek is reasonable.

Teleconnection data for three oceanic indices, the Arctic Oscillation (AO), PDO, and Oceanic Niño Index (ONI), were obtained from the sources described in Table 2. For each of these teleconnections, we calculated the monthly mean indices from the period December to March to create a winter index for a particular year (i.e., December of 1917 to March of 1918 were averaged to a single value representing winter 1918).

Journal of Geophysical Research: Earth Surface

10.1029/2023JF007154

Table 2
Measured and Derived Climate and Weather Variables Used in the Avalanche-Climate Modeling Analysis (Described in Section 2.5)

Variable	Description	Frequency of source data	Period of record analyzed	Source
Arctic Oscillation Index (AO)	Index of daily 1,000 mb height anomalies poleward of 20°N mapped to the loading pattern of the AO from 1979 to 2000 (Thompson & Wallace, 1998)	Monthly	1917–2020 (December–March)	JISAO
Oceanic Niño Index (ONI)	Ensemble rolling 3-month average temperature anomaly of east-central tropical Pacific surface waters since 1850	Monthly	1917–2020 (December–March)	Webb and Magi (2022)
Pacific Decadal Oscillation Index (PDO)	Leading principal component of North Pacific monthly sea surface temperature variability	Monthly	1917–2020 (December–March)	NCEI
Maximum temperature (T_{max})	Maximum daily temperature (°C)	Daily	1917–2020	GHCN Annex Creek (elev. 28 m)
Minimum temperature (T_{min})	Minimum daily temperature (°C)	Daily	1917–2020	GHCN Annex Creek (elev. 28 m)
Precipitation (prcp)	Cumulative precipitation (mm)	Daily	1917–2020	GHCN Annex Creek (elev. 28 m)
Cumulative snow (snow)	Cumulative snowfall (mm)	Daily	1917–2020	GHCN Annex Creek (elev. 28 m)

Note. JISAO = Joint Institute for the Study of the Atmosphere and Ocean, NCEI = National Oceanic and Atmospheric Administration National Centers for Environmental Information, GHCN = National Oceanic and Atmospheric Administration Global Historical Climatology Network.

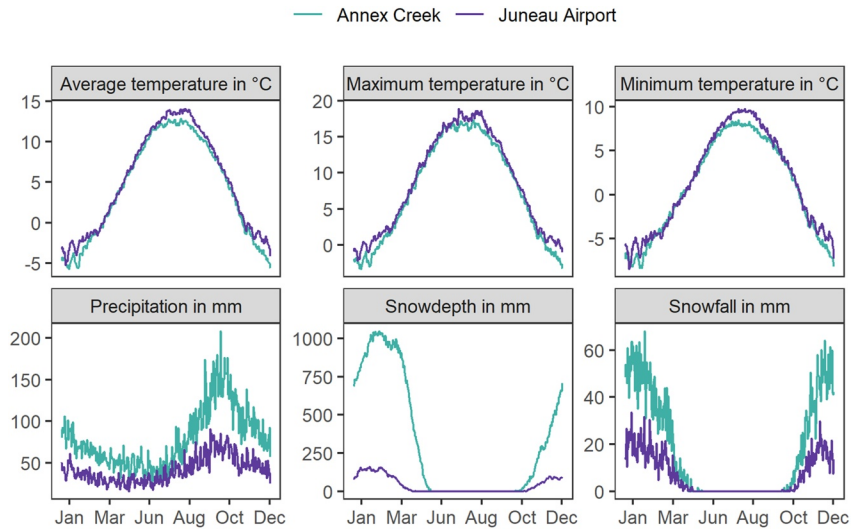

Figure 2. Average daily climate variables measured at two locations (see Figure 1) in the Juneau area, southeast Alaska. Periods of record are approximately 1917–2021 for Annex Creek and 1936–2021 for the Juneau Airport.

For the AO, we obtained monthly mean AO indices from the Joint Institute for the Study of the Atmosphere and Ocean (JISAO) (http://www.atmos.colostate.edu/davet/ao/Data/aoindex.html), as described in Thompson and Wallace (2000). This data set covers the period of 1899–2002. To extend the AO period through the extent of our dendrochronology time series, we extended this AO time series using monthly average AO indices from 1950 to 2020 from the NOAA Climate Prediction Center (CPC, https://www.cpc.ncep.noaa.gov/products/precip/CWlink/daily_ao_index/monthly.ao.index.b50.current.ascii). To extend the AO time series, we examined the Pearson correlation coefficient between the JISAO AO indices and the CPC AO indices over the extent of the overlap period (1950–2002) and found the two time series to be in good agreement ($r = 0.97$). We fit an orthogonal regression model between these two time series and used the model intercept (intercept = −0.13) to apply a correction factor to monthly CPC AO indices from 2002 to 2020. In this way, we obtained a complete AO index time series from 1899 to 2020 with the period 2002–2020 generated using this correction factor (Figure S2 in Supporting Information S1).

We calculated emergent variables from climate data using daily records obtained from the GHCN (GHCN, 2022). We calculated total precipitation and total snowfall for each month November through March as the sum of daily precipitation (e.g., prcp_Jan) and snowfall (e.g., snow_Jan).

2.5. Avalanche and Climate Statistical Analysis

We used a glm to fit a binomial regression (logit link function) predicting a binary outcome (LMA or no LMA) from our continuous predictor variables. Generalized linear models are an extension of linear regression where the response variable is modeled using a link function rather than across a continuous distribution. This allows for modeling of non-normally distributed data such as Poisson distributions (e.g., count data) or binomial data (presence/absence). In this case, we modeled a binary outcome (LMA or no-LMA); thus, the model used a logit or binomial link function to predict probabilities of the occurrence of 0 (no-LMA) or 1 (LMA) using the climate variables discussed above (e.g., prcp_Jan).

We aggregated the common reconstructed LMA years from the subregions ($n = 82$) to provide a larger sample size when compared to the reconstructed LMA years across the region ($n = 38$). Using the aggregated years from the subregions allowed for a more conservative estimate of the number of years associated with LMAs, which is preferable to underestimating years when assessing natural hazards with societal impact and allowed for a more robust statistical analysis. We used the linearity of continuous predictor variables against logit-transformed LMA outcomes, which we assessed visually. Initial model predictor variables included ONI, PDO, AO, monthly precipitation January through March (prcp_Jan, prcp_Feb, prcp_Mar), and monthly snowfall January through March (snow_Jan, snow_Feb, snow_Mar) (Table 2). To ensure models were not overfit, we used a backward

Table 3
Proportions of Signals in Each Growth Disturbance (GD) Class

	Class 1	Class 2	Class 3	Class 4	Class 5
Scar	0.27	0.03	0.01	0.01	0.04
Reaction Wood	0.19	0.90	0.95	0.93	0.71
Growth Suppression	0.04	0.07	0.01	0.01	0.00
Traumatic Resin Ducts	0.11	0.05	0.06	0.10	0.30
Observed/Historical Record	0.64	0.00	0.00	0.00	0.00

Note. Note that proportion totals for each class are greater than 1 because multiple signals can exist for any given year (e.g., scar with associated reaction wood).

stepwise regression procedure to iteratively eliminate variables by minimizing the Akaike Information Criteria (AIC_c) value. We also examined multicollinearity for the full model by calculating the variance inflation factor.

3. Results

3.1. Avalanche Chronology Reconstruction

Using a strategic sampling plan, we collected 434 cross sections from 426 unique trees throughout six avalanche paths in the study region. This resulted in 2706 identified GDs due to avalanches, with 261 classified as C_1, 687 as C_2, 643 as C_3, 461 as C_4, and 199 as C_5 (Table 3). Observations and death dates of sampled trees comprised the majority of the GDs in C_1, and various representations of reaction wood were the majority of signals in C_2 through C_5. The mean age of trees sampled was 199 years (Figure 3a), and the most prevalent species was *Tsuga mertensiana* (mountain hemlock) (Figure 3b).

The number of samples (i.e., trees alive in each year) able to record avalanche disturbance generally increases through time in most of the individual avalanche paths (Figure 4). Deviations from this pattern exist in the South

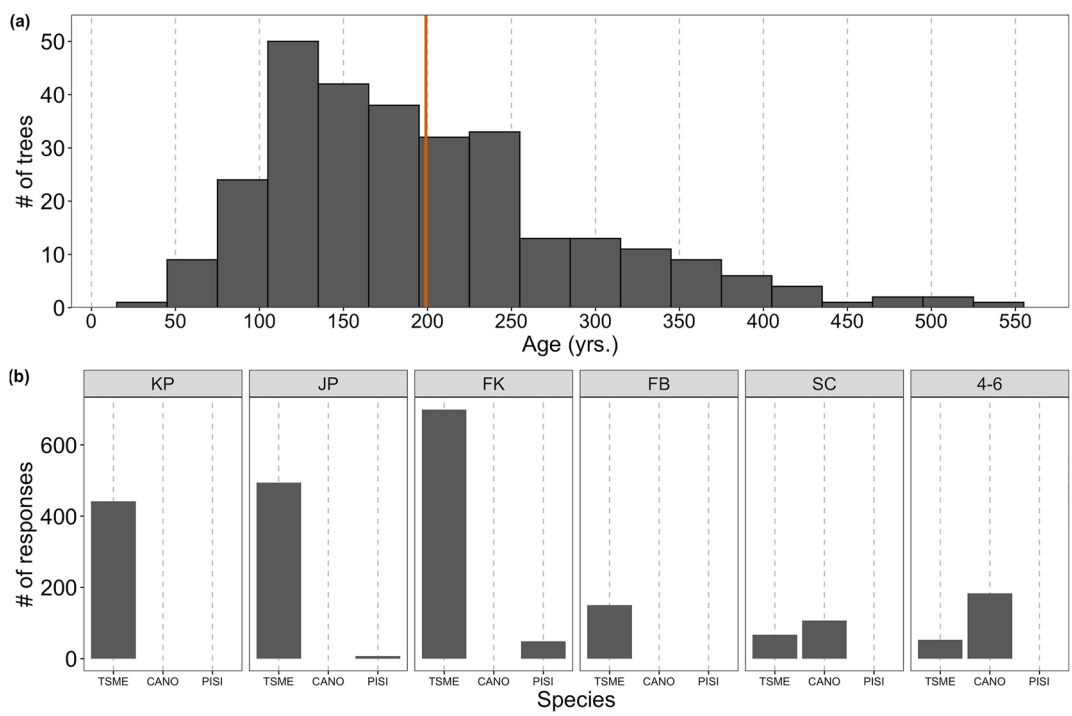

Figure 3. Histograms of (a) sample age (vertical red line represents mean age), and (b) sampled species for each avalanche path (labeled at top): mountain hemlock (*Tsuga mertensiana*; TSME), Alaska yellow-cedar (*Callitropsis nootkatensis*; CANO), and Sitka spruce (*Picea sitchensis*; PISI).

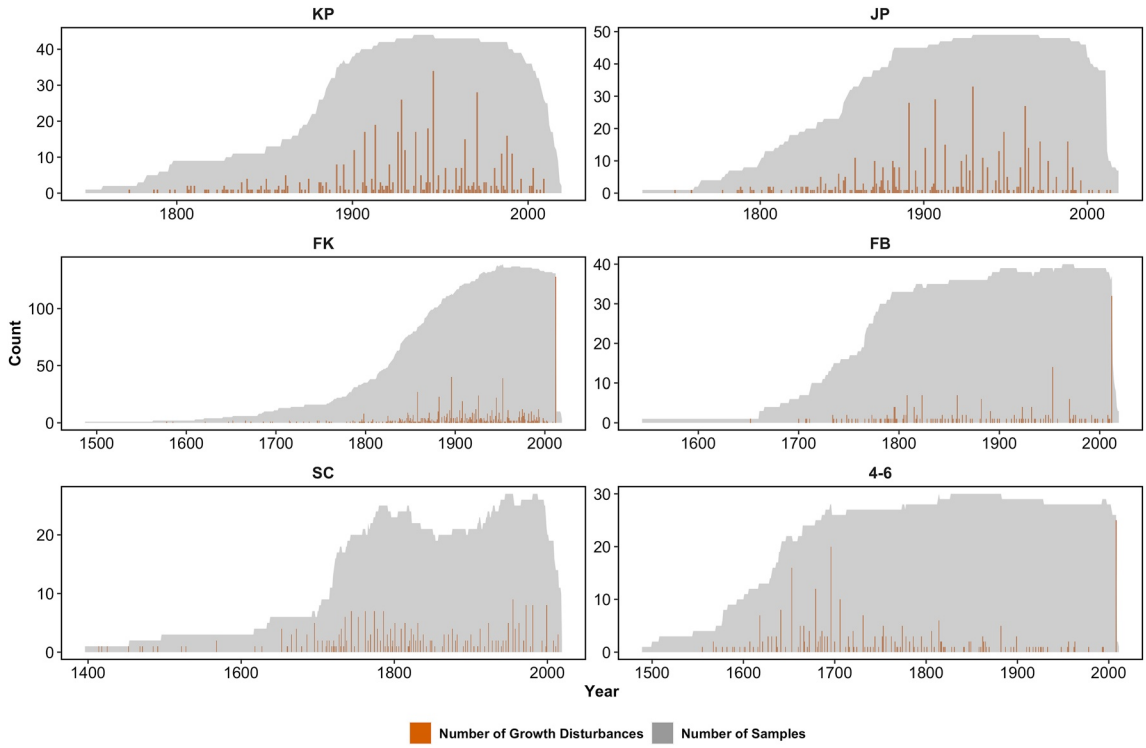

Figure 4. The number of trees alive and able to record avalanche disturbance (gray area plots) and the number of growth disturbances (orange columns) for all six individual avalanche paths in this study. Note the variable *x*- and *y*-axes for each plot. Avalanche path names: KP = Kensington Portal, JP = Jualin Portal, FK = Fish Creek Knob, FB = Fruit Bowl, SC = South Crater, 4–6 = 4–6 Diverter. Gray lines represent the Fish Creek sub-region, Blue lines represent the Kensington sub-region, and green represents the Snettisham sub-region.

Crater and 4–6 paths. In South Crater, the sample size increases until the late 18th century, decreases until the mid-1800s, then generally increases again. The sample size in path 4–6, also in the Snettisham sub-region, increases and then plateaus with minor changes from the 1700s to the modern era. These two paths also contain the smallest number of trees alive per year despite our efforts to collect over 50 and 60 samples in 4–6 and South Crater, respectively.

3.2. Return Periods Across Scales

Using a multi-step process to distinguish avalanche signals from noise, we reconstructed avalanche chronologies for individual avalanche paths, subregions, and the entire study region (Table 4 and Figure 5). Across all six avalanche paths, we identified 128 avalanche events. On the individual path scale, Fruit Bowl (FB) in the Fish Creek subregion exhibited the largest median RI of 30 years and the two avalanche paths in the Kensington subregion (Kensington Portal and Jualin Portal (JP)) the smallest RIs (5 and 6 years, respectively). The Kensington subregion avalanche paths also contain the greatest number of years with LMAs in the reconstructed chronology (30 and 29 years). Fruit Bowl, on the other hand, contains the fewest number of years with LMAs (7 years), and 4–6 contains the greatest interval between any two avalanche years in the chronology with a maximum RI of 126 years. The RIs of FB and FK significantly differ and are the only two paired paths within each subregion that differ (Table S2 in Supporting Information S1, $p < 0.001$).

We reconstructed 37 years with LMA activity in the Kensington subregion, 33 years in the Snettisham subregion, and 23 years in the Fish Creek subregion. The reconstructed chronology for the entire region contained 38 years associated with LMAs. The total common reconstructed LMA years across subregions are 82 from 1720 to 2018, 50 years from 1850 to 2018 (period of ONI and avalanche analysis) and 31 years from 1918 to 2018 (period of full climate analysis).

The subregion with the greatest median RI of years with LMAs was Fish Creek (10 years) followed by Snettisham (9 years) and then Kensington (4 years). The subregion with the greatest maximum RI was Snettisham (73 years).

Table 4
Avalanche Chronologies and Return Interval (RI) Statistics of All Six Avalanche Paths in the Region

Subregion	Kensington		Fish Creek		Snettisham	
Path	KP	JP	FK	FB	SC	4–6
Aval Years	**1837**	**1837**				
	1840	1848				
	1851	1858				
	1862	1870	1798			
	1870	1875	1825			
	1875	1881	1847		1728	
	1891	1882	1848		1731	
	1895	1885	**1858**		1736	1618
	1901	**1891**	1871		1744	1627
	1907	**1895**	1881		1753	1631
	1913	**1901**	1882		1762	1636
	1921	**1907**	1894	1808	**1774**	1641
	1926	**1913**	1896	1823	1786	1653
	1928	1923	1905	**1858**	1801	1662
	1930	1926	1908	1882	1814	1666
	1936	**1928**	1919	1953	1831	1679
	1939	**1930**	1923	1970	1865	1696
	1943	**1936**	1926	**2012**	1871	1706
	1946	**1939**	1941		1923	1731
	1949	1946	1946		1949	1753
	1953	1949	1949		1955	**1774**
	1959	**1959**	1953		1963	1814
	1962	**1962**	1972		1972	1882
	1964	**1964**	1975		1981	2008
	1971	**1971**	1985		1999	
	1981	1976	1993		2014	
	1985	1981	**2012**			
	1988	**1988**				
	1991	**1991**				
	2003					
# Of aval. years	30	29	24	7	21	17
POR (raw samples)	1748–2019	1728–2019	1487–2019	1544–2019	1396–2019	1489–2011
RI median	5	6	9	30	11	12.5
RI mean	5.72	5.5	9.30	34.00	14.30	24.38
RI min.	2	1	1	15	3	4
RI max.	16	12	27	71	52	126

Table 4
Continued

Subregion	Kensington		Fish Creek		Snettisham	
Path	KP	JP	FK	FB	SC	4–6
1/RI	0.2	0.17	0.11	0.03	0.09	0.08
σ	3.47	2.98	7.22	20.90	11.53	31.72

Note. Avalanche years in bold indicate years identified in two avalanche paths in the subregion. Underlined avalanche years indicate years in common in at least one path from at least two of the three subregions. Avalanche years in italics indicate years in common in three or more avalanche paths. 1/RI refers to the probability of an avalanche occurring in that avalanche path in any given year, and $\boldsymbol{\sigma}$ represents the standard deviation of the RI. The period of record (POR) for each path represents the earliest inner year to the most recent outer year of all the samples in the path. The RI was calculated on the return interval of avalanche years.

The range of RI is greatest at Snettisham and more tightly clustered in Kensington. Snettisham and Kensington are the only subregions that exhibit a significant difference in RIs (Table S2 in Supporting Information S1, $p < 0.01$). The median RI of years with LMAs across the broader study region is 9 years. However, the RI for the entire region exhibits a bimodal distribution with peaks at approximately 4 years and another at 9 years.

3.3. Monthly Climate Variables and LMAs

The monthly minimum, mean, and maximum winter (November through April) temperature (°C) profiles for years with LMAs exhibit similar patterns when compared to temperature profiles for years without LMAs across the region (Figure 6 and Figure S3 in Supporting Information S1). The only significant difference in total monthly precipitation between LMA and non-LMA years exists in February (Figure S4 in Supporting Information S1). However, the precipitation pattern shifts in January, where cumulative monthly precipitation increases in LMA years before decreasing again through the rest of the winter, but median precipitation generally decreases during non-LMA years. Cumulative snowfall (mm), on the other hand, is greater every month during years with LMAs compared to non-LMA years.

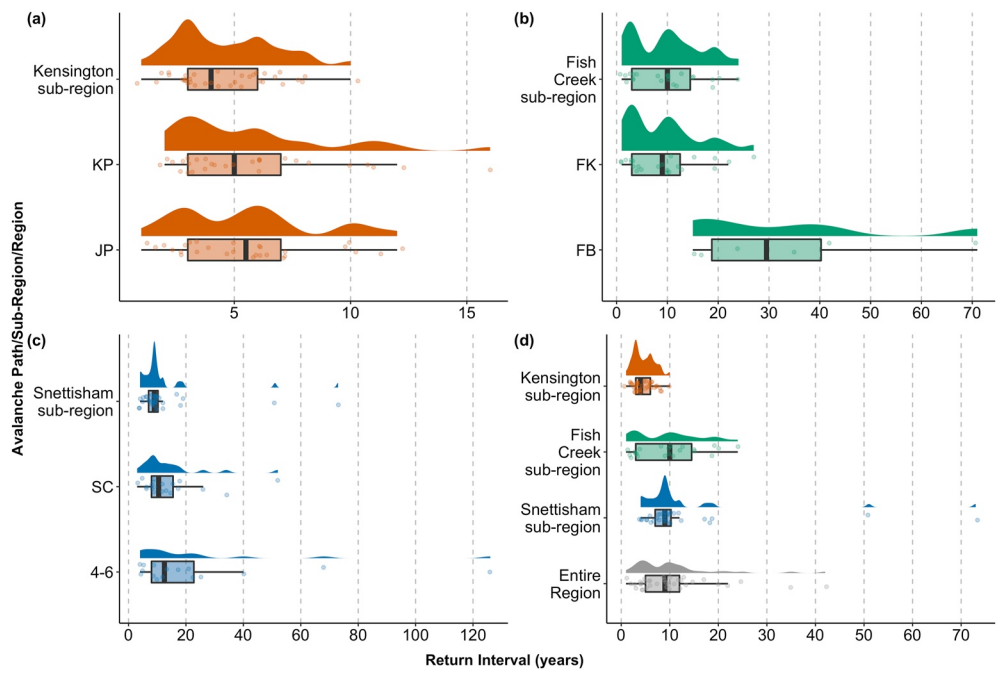

Figure 5. Raincloud plots for the individual paths within each of the three subregions (a–c) and the subregions compared to the entire study region (d). Note the different *x*-axis scale for each subregion. Kensington subregion: KP = Kensington Portal, JP = Jualin Portal; Fish Creek subregion: FK = Fish Creek Knob, FB = Fruit Bowl; Snettisham subregion: SC = South Crater, 4–6 = Diverter 4–6. Entire region represents these six paths aggregated.

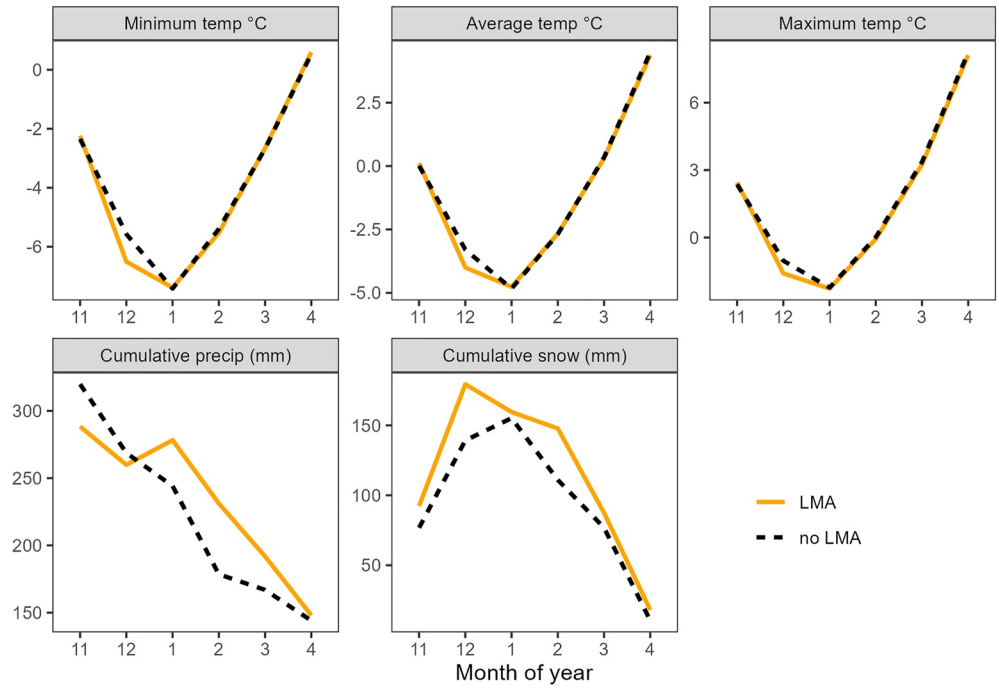

Figure 6. Summary of monthly climate variables (November through April) grouped years with large magnitude avalanches (LMA, solid gold line) and years without large magnitude avalanches (no LMA, dashed black line) throughout the region.

3.4. Generalized Linear Model of Avalanche Years

Using a glm to fit a binomial regression allowed us to predict a binary outcome (LMA or no LMA) from our continuous independent variables. Results of the glm indicate ONI, February precipitation, and March precipitation to be significant predictors of years associated with regional LMAs (Table 5). Variance inflation factor values for each predictor variable were all less than 1.6, indicating that the predictor variables were not significantly correlated.

The logistic regression model coefficients for January and February precipitation ($\beta = 0.001$ and 0.001, respectively) indicate that the odds of a LMA year increase by 0.1% for every cumulative unit increase in precipitation for both months (Figures 7a and 7b). Cumulative precipitation in February exhibits a non-linear directional influence on whether a year is associated with LMAs or not, while the direction of influence from precipitation in January is linear.

Closer inspection of ONI as a statistically significant predictor variable ($\beta = -0.65$, $p = 0.02$) in the logistic regression model shows a negative coefficient ($\beta = -0.65$) indicating that the odds of a LMA year decrease by 48% for each unit increase in the ONI (El Niño; Figure 6c). Through the full time series of the ONI index associated with our reconstructed regional avalanche chronology (1850–2018), there are 53 years of positive (El Niño) ONI, 49 years of negative (La Niña), and 70 neutral years. Of those years, LMA activity occurred in either a positive (El Niño, 11 years) or negative (La Niña, 14 years) phase 25 times and during neutral conditions (−0.5 to 0.5) 25 times (Figures 8a and 8b).

Table 5
Results of the Generalized Linear Model Fit Predicting Binary Outcomes of Avalanche Year or No Avalanche Year and Fit Using a Logit Link Function

	Estimate	Standard error	z value	p-value
Intercept	−3.72	0.97	−3.85	0
ONI	−0.65	0.28	−2.32	**0.02**
prcp_Feb	0.001	0.00	2.60	**<0.01**
prcp_Mar	0.001	0.00	2.13	**0.03**

Note. A backward stepwise regression procedure was performed using AIC to select the most parsimonious set of predictor variables from the full model. P-values are calculated using Walds tests, with significance at the $\alpha = 0.05$ level (bold).

The overall model (hereafter, naïve model) accuracy is 72% when probability outcomes >0.5 are predicted to be years associated with LMAs and outcomes ≤0.5 are predicted to be years without regional LMA events. We implemented a supervised probability range when assessing the probability of a given year being one associated with or without LMAs (Table 6 and Figure 9a). When we classify outcome probabilities >0.60 as confident it is a large magnitude year and below 0.25 as confident it is a non-LMA year model performance improves (83% and 85%, respectively) (Figure 9b). The model performs poorly when the probability of outcome is between 0.25 and

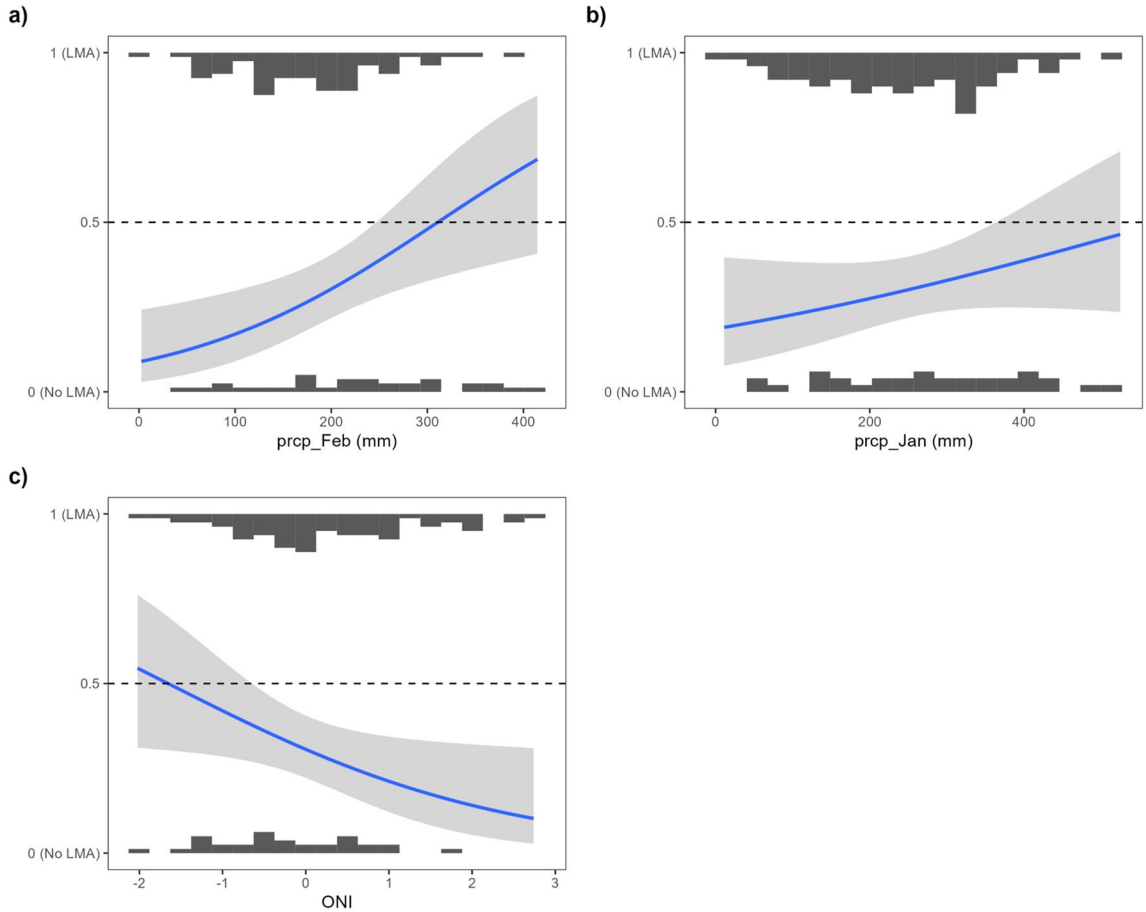

Figure 7. Single variable logistic regression models show the directional influence of the three variables selected for the final model: (a) monthly cumulative February precipitation (mm), (b) monthly cumulative January precipitation (mm), and (c) Oceanic Niño Index. Histograms at the top and bottom of each plot represent the density of observations along the *x*-axis—relative densities can be inferred within each panel but should not be compared between panels. Large magnitude avalanche (LMA) = years with regional LMA events, non-LMA = years without regional LMA events. The *y*-axis denotes model output odds (1 = LMA and 0 = no LMA) where the horizontal dashed line represents equal odds of both outcomes. The dashed line represents the 0.5 probability level.

0.60 (hereafter, undecided) with a designated threshold of 0.5 (>0.5 = correct and <0.5 = incorrect) and with an accuracy of 56%.

4. Discussion

4.1. Avalanche Chronology and Return Frequency

The 2706 GDs identified in this study from 426 trees across a large spatial extent allowed us to identify 82 years with regional LMA activity from 1720 to 2018. This large sample size of GDs consisted mostly of C_2 and C_3 signals in the tree ring samples. While signals rated C_1 represent the highest quality, they represent only 11% of the GDs identified in this data set. C_2 and C_3 quality samples, on the other hand, comprise 59% of the data set. The small number of C_1 samples could potentially be attributed to the relatively rapid decomposition of mountain hemlock wood, which comprised the majority of samples in our data set, compared to Alaska yellow-cedar, which is far more resistant to rot and decay (Hennon et al., 2002). Thus, the overall rate of decomposition of dead and down trees (particularly hemlock) in this wet maritime climate likely prevented us from confidently classifying some signals as C_1. This differs from other studies where C_1 signals are the most abundant category of avalanche signals (Favillier et al., 2018; Peitzsch, Hendrikx, et al., 2021). However, the large overall number of GDs and the weighting process we employed (see Section 2.3) allowed us to confidently reconstruct the avalanche chronology in the study region. This use of cross sections and a large sample size also allowed for a complete assessment and a comparison against other samples where reaction wood may exist in some, but not other, samples for consecutive years; thus, reducing the ability to record avalanche activity (Gratton et al., 2020).

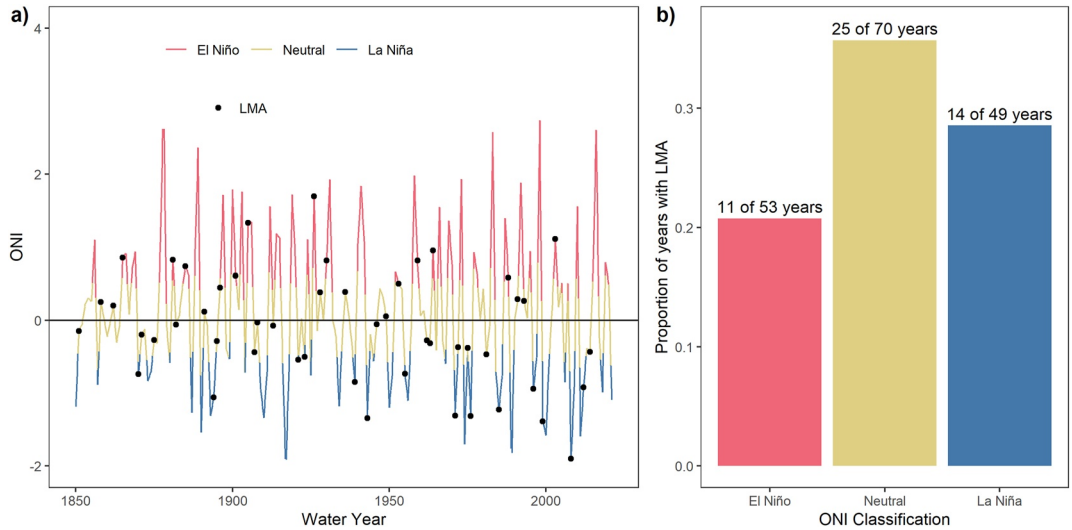

Figure 8. (a) Oceanic Niño Index (ONI) since 1850, with associated El Niño (warm), La Niña (cold), and la nada (neutral) phases. Years with large magnitude avalanche (LMA) events in southeast Alaska determined by dendrochronology reconstruction are shown as points along the time series. (b) proportion of years for each ONI category with LMA events.

The RIs of LMAs within each individual path across the region exhibit a large range (1–126 years). Fruit Bowl exhibits the greatest minimum RI at 15 years while the RIs in the other 5 paths range from 1 to 4 years. The mean slope angle of the FB starting zone is 33 degrees which may act as a potential topographic influence on avalanche release and subsequent higher RI in this path. Jualin and Kensington paths in the Kensington subregion exhibit the most frequent median (and mean) RI likely due to regular avalanche mitigation measures beginning in 2007–2008 to protect the Kensington gold mine, which lies directly downslope of these paths. Prior to this concentrated management effort, infrequent mitigation occurred in these paths. While it is possible that artificial avalanche mitigation resulted in some LMA years in our reconstruction, this fails to account for a consistently frequent RI from the early 1800s to the early part of the 21st century when mitigation was not as frequent. This more frequent LMA activity could also be explained by the topographic characteristics of these two paths; JP and KP are the smallest in area (0.03 and 0.05 km^2, respectively) and vertical distance (230 and 360 m, respectively). Therefore, it is possible that more frequent avalanches smaller than size D3 on the destructive scale could cause mechanical damage to the sampled trees and register as avalanche signals in these two paths (Corona et al., 2012). However, we sampled dead and downed trees in the lower most part of the runout zone in both paths where the path length is 230 and 360 m. This exceeds the typical path length for size D2 avalanches on the destructive scale (Greene et al., 2016), suggesting that the avalanche signals in these paths represent LMAs as defined in this study. Kensington also experienced landscape disturbance (i.e., logging) that limits the sample depth prior to the mid-19th century.

Similar to other avalanche studies using dendrochronological data, the number of trees alive each year in each avalanche path generally increases in the individual avalanche paths in this study (Corona et al., 2012; Favillier et al., 2023). Exceptions include the two paths in the Snettisham region. In South Crater, specifically, the number of trees alive each year and subsequent ability to record avalanche activity in their rings increases and decreases

Table 6
Supervised Classification Categories Based on the Modeled Outcome Probability and Reconstructed Regional Avalanche Chronology for Each Year

Model outcome probability and reconstructed result	Supervised classification	Accuracy
Probability ≥0.6 and reconstructed LMA year	Correct Confident LMA	83%
Probability <0.25 and reconstructed non-LMA year	Correct Confident non-LMA	85%
Probability ≥0.25 AND <0.5 and reconstructed non-LMA year	Correct Undecided	56%
Probability ≥0.5 AND <0.6 and reconstructed LMA year	Correct Undecided	
All else	Incorrect	NA

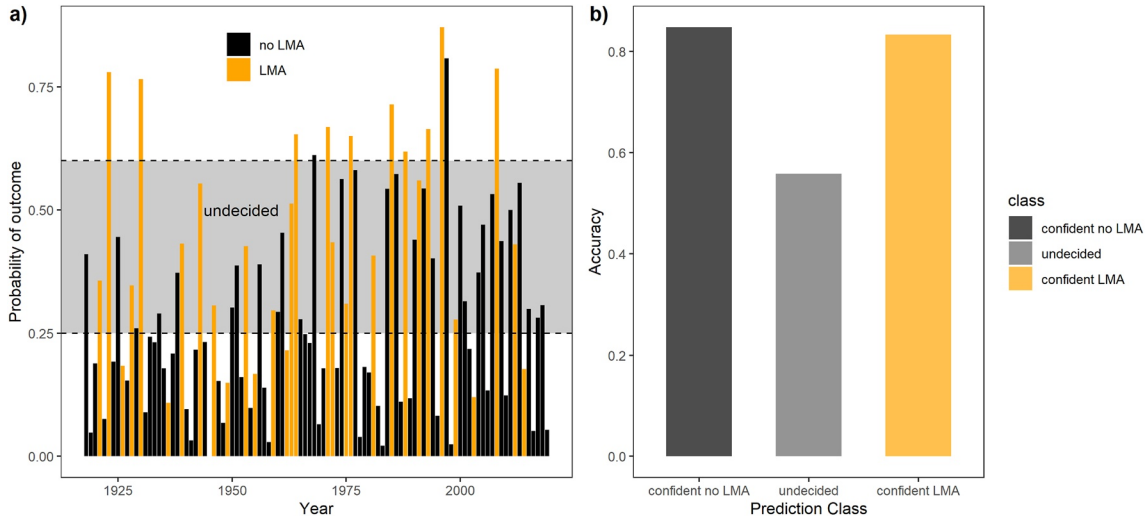

Figure 9. (a) Predictions (probabilities) of the model containing Oceanic Niño Index, precip_Feb, and precip_Mar for each year. Observed outcomes are presented as the color of the bar (black = no LMA, yellow = LMA) in each year. The gray shaded area represents the range of probabilities between 0.25 and 0.60 and classified as "undecided". We classify areas above this shaded area (0.61–1.00) as "confident LMA" and areas below (<0.25) as "confident no LMA". (b) Accuracy improved for predictions above and below the undecided region.

throughout the chronology. The number of trees able to record avalanches in 4–6 increases and then generally flattens. The maximum number of trees alive in any given year in these paths is also smaller than the other four paths in the region. This likely influenced the RIs for these individual paths. Observations indicate large avalanches in both avalanche paths in the Snettisham runout to the ocean. Therefore, large to historic-sized avalanches during the 20th century removed trees, deposited debris into the ocean, and limited the available material for sampling.

Additionally, in 1920 in the Snettisham area Alaska Pulp and Paper Company purchased a large timber sale and constructed a small pulp mill at Port Snettisham. In 1967, construction began on the first component of the Snettisham Hydroelectric Facility. Combined, these human disturbances likely removed potential material for sampling as the electric transmission lines traverse through these avalanche paths in the Snettisham area.

The significant difference in RIs between FK and FB highlights the potential difference in snowpack structure due to aspect. Fish Creek Knob faces southwest while FB is east facing. Subtle differences in snowpack structure and localized winds can explain why these two paths are the only paths that exhibit different RIs within any given subregion. Similarly, Gratton et al. (2020) found differences in avalanche activity by aspect due to varying meteorological drivers using a tree-ring reconstructed data set, and Reuter et al. (2015) found aspect to be a primary driver of snowpack instabilities.

The bimodal distribution of RIs across the entire region indicates a potential for regional LMAs every 4–9 years. The variability of median RIs across the subregions supports this and suggests that multiple subregions are necessary to reconstruct and evaluate regional LMA activity. This is particularly true within southeast Alaska where the high-latitude maritime climate exhibits very strong air temperature gradients that influence the form (liquid vs. solid) and amount of precipitation as a result of microtopographic influences and the proximity to atmospheric circulation originating from either the Gulf of Alaska to the west or the extensive icefield complex to the east (Lader et al., 2020; Shanley et al., 2015). Overall, our results illustrate the interannual variability within each avalanche path within a given region and highlights the importance of sampling multiple paths when attempting to examine LMA activity at a regional scale (Favillier et al., 2023; Germain et al., 2010; Giacona et al., 2021; Hebertson & Jenkins, 2003; Martin & Germain, 2017; Peitzsch, Hendrikx, et al., 2021). This sampling strategy also aligns with regional climate and synoptic meteorological influences on snowpack and subsequent avalanche activity (Eckert, 2010; Giacona et al., 2021; Peitzsch, Pederson, et al., 2021).

4.2. Climate Associations With Avalanche Activity

We examined specific climate variables and atmospheric teleconnection indices for relationships with LMA activity in the study area. Overall, monthly air temperature patterns suggest November and December temperature is

similar in years with and without LMA activity across the region. Median monthly precipitation is not significantly different between LMA and non-LMA years except for February. However, it is worth noting the differences in precipitation patterns. The monthly median precipitation in years with LMAs increases from December to January leading to a significant difference with non-LMA years in February. Years with LMAs exhibit significantly greater cumulative February precipitation, suggesting a scenario of a relatively shallow early winter (November and December) snowpack followed by an increase in storminess and precipitation across the region in the latter part of the winter. Early season shallow snowpacks limit the runout extent and associated size of avalanches capable of impacting trees in avalanche runout zones, consistent with infrequent early season LMA activity due to a reduced volume of available snow (Bartelt et al., 2012; Eckert et al., 2013). However, early season shallow snowpacks often lead to persistent weak layer development, and, when combined with sufficient storms later in the winter, increase the probability of large deep slab avalanches (Marienthal et al., 2015). Overall, this finding suggests that the climatological differences between years with and without LMAs generally develop from January onward and are largely independent of early winter (November and December) temperature and precipitation.

To further elucidate climate drivers of LMA activity in southeast Alaska, we used a logistic regression model and found ONI, February precipitation, and March precipitation to be significant predictors of years with LMA activity. These results indicate that late-winter (February and March) precipitation is the primary driver of LMA activity in this region; however, the relationship with ONI also suggests that there is an interaction with winter temperature, which is significantly warmer in southeast Alaska during the positive phase of the ONI (Fleming & Whitfield, 2010; Papineau, 2001). Air temperature plays a substantial role in the accumulation of winter snowpack in our study region because the long term (1991–2020) average winter (November through March) temperature is within 0.5°C of the freezing point of water (NOAA, 2022). As a result, small changes in winter temperature associated with shifts in the state of the ONI can change the form of precipitation (liquid vs. solid) during winter months. Within southeast Alaska, there are few long-term records of snow accumulation, and fewer still at mid- and high-elevation locations where avalanches start. However, the influence of the ONI on snowpack accumulation in the Coast Mountains is evidenced by the fact that the positive (warm) phase of the PDO, a teleconnection with similar regional signatures to El Niño/Southern Oscillation, is associated with a significant increase in winter streamflow regionally (from increased liquid precipitation during winter) and a corresponding decrease in regional summer streamflow (from lower winter snow accumulation (Neal et al., 2002)).

These empirical observations are consistent with our results showing that small perturbations in winter temperature as reflected by the ONI signals in the logistic regression model had a significant impact on the probability of LMAs. A large percentage change in the odds of LMA activity in southeast Alaska (48%) occurs with a single unit change in ONI, indicating the substantial influence of temperature on precipitation type in February and March, which influences avalanche activity. In northwest Montana, USA, Dixon et al. (1999) report a relationship between El Niño years and a decrease in avalanche activity. Similarly, Peitzsch, Pederson, et al. (2021) show a short-term variability component in their climate data set is driven by ENSO and this component is a significant predictor of avalanche years in the northern Rocky Mountains, United States. Germain et al. (2009) also found more than a third of the years with LMAs in their data set in eastern Canada occurred during El Niño years.

The influence of seasonal temperature regimes on LMA activity has broad implications for modeling avalanche activity in maritime regions where temperature is an important control on snow accumulation compared to interior, continental environments (Mote et al., 2018; Pederson, Gray, Woodhouse, et al., 2011). Our tree ring constructed chronology of LMA shows that neutral ONI followed by the La Niña (cold) phase comprises the greatest proportion of years with LMA activity in our data set, while winters exhibiting El Niño conditions are associated with a lower proportion of years with LMA activity. This is consistent with the idea that, while precipitation is an important predictor of LMA years, temperature dictates the precipitation type (rain vs. snow) falling in the Coast Mountains of southeast Alaska. Thus, temperature can be seen to modulate the positive relationship between precipitation and LMA years in coastal environments, as in Gratton et al. (2020), with the frequency of large, snow-producing storms increasing during the cold phase of the ONI. Similarly, Martin and Germain (2017) and Keylock (2003) demonstrate the importance of atmospheric circulation patterns on regional avalanche patterns in the Presidential Range of New Hampshire, the United States, and Iceland, respectively. These results also align with several studies showing a decrease in the probability of avalanches as snowpack declines and temperature warms as well as a decrease in avalanche runout extent (Castebrunet et al., 2012; Eckert et al., 2013; Giacona et al., 2021; Peitzsch, Pederson, et al., 2021).

4.3. Model Performance

Logistic regression has been used to investigate avalanche activity and associated weather and climate influences. Gauthier et al. (2017) conclude that logistic regression is a valuable tool when examining meteorological drivers of avalanche activity in the maritime climate of eastern Canada. Hebertson and Jenkins (2003) found logistic regression a useful technique to demonstrate that January snowfall was a significant driver of avalanche activity in the Wasatch Range, Utah, USA, but found that the model failed to explain a substantial amount of variability in the data set. They report a small sample size of tree-ring data from individual paths and a lack of complete, long-term climate data set as limitations to their study. Here, we leverage a large ($n = 435$) data set of tree-ring records and long-term climate records to improve the ability of a logistic regression model to accurately predict avalanche probability. We use monthly and seasonal temperature, precipitation, and snowfall as local climate variables to account for the influence of short-term climate variability as well as teleconnection indices (ONI, PDO, AO) to account for mesoscale climate influences. Using these two general types of climate drivers allows us to relate regional avalanche activity and climate at the appropriate spatio-temporal scale for tree-ring based avalanche reconstructions.

In our study, the glm outcome indicates reasonable accuracy predicting LMA years (72%) using a cutoff of 0.5 where probability outcomes >0.5 are predicted to be years associated with LMAs and outcomes ≤0.5 are predicted to be years without regional LMA events. The accuracy of prediction in the confident LMA class was high (83%) but represented a small minority of LMA observations over the entire period of record. The probability of outcome between 0.25 and 0.6 is where the model struggles to properly classify years associated with LMA activity or years without LMA activity. Therefore, we implemented a supervised probability range, which improved the performance of our model. Collectively, our findings indicate that a logistic regression model can provide useful information about the climate drivers of years with LMAs when the probabilities are partitioned in a supervised way. The limitation, of course, is distinguishing between whether conditions associated with probabilities in the 0.25 to 0.6 range will result in LMA or not. The lack of accuracy in predicting probabilities in this range could be attributed to the sensitivity of the ONI signal in the model. In particular, the model struggles to predict LMA activity when the influence of temperature on the form of precipitation is difficult to discern from the ONI (i.e., temperature is not clearly warm or cold). In this context, our model can provide reliable information for the higher and lower probability ranges for LMA years. By identifying February and March precipitation and ONI as drivers of LMA activity, we provide information that can be used operationally to plan avalanche mitigation resources more effectively. However, the interaction of weather and snowpack structure on daily to seasonal time scales is important when forecasting avalanches (Morin et al., 2019). Therefore, using a finer temporal scale of weather variables (e.g., daily), while also including snowpack structure variables, may help improve the accuracy of the "undecided" range and address the limitations of the model (Gauthier et al., 2017). Additionally, the nature of tree growth and our tree-ring record limits the resolution of avalanche signals to an annual scale, and, as such, finer scale avalanche records could further increase model performance. However, despite these limitations, this study aimed to examine the climate-avalanche relationship in southeast Alaska, and our findings shed light on important climate variables and physical processes associated with LMA years throughout the study area. These results can be used to help inform long-term infrastructure planning and avalanche mitigation operations, particularly in an urban avalanche context such as Juneau, Alaska.

5. Conclusions

We reconstructed a LMA chronology from 1720 to 2018 using an extensive tree-ring data set from six avalanche paths in southeast Alaska. We identified 82 years with LMA activity common throughout the study's three sub-regions. Using a suite of climate and atmospheric teleconnection variables, we examined avalanche-climate relationships from 1850 to 2018 that included 50 years identified as LMA years. Our results show variable return period frequencies throughout the six individual avalanche paths, but, when aggregated to sub-regions, the median return period becomes more consistent across three sub-regions. The RIs for the entire region exhibit a bimodal distribution suggesting a median RI of 9 years across the region but a secondary peak at 4 years.

Our analysis of the relationships between LMA activity and climate revealed an important influence of mid-winter precipitation and temperature. A glm fit with binomial regression (LMA vs. non-LMA year) showed February and March precipitation and the ONI to be statistically significant predictors of LMA activity within a given year. The probability of LMA activity increased with February and March precipitation. Years with positive (warm)

ONI values, a proxy for short-term temperature variability in our data set, were associated with a greater probability of a year being one without LMA activity. Overall, our results suggest that the climatological differences between years with and without LMAs generally develop from January onward and are largely independent of early winter (November–December) temperature and precipitation. The limitations of the predictive capabilities of the model can likely be attributed to a lack of snowpack structure variables, since avalanche activity heavily depends on snowpack stability. In this study, however, our objective was to examine climate-avalanche relationships in southeast Alaska, and we demonstrate that these results can be used to help inform long-term infrastructure planning and avalanche mitigation operations.

Disclaimer

Any use of trade, firm, or product names is for descriptive purposes only and does not imply endorsement by the U.S. Government.

Data Availability Statement

Data for this work can be found in Peitzsch et al. (2023): https://doi.org/10.5066/P9LPZPJP.

Acknowledgments
The U.S. Geological Survey Alaska Climate Adaptation Science Center provided funding for this project. Coeur Alaska, Eaglecrest Ski Area (Brian Davies), and the City and Borough of Juneau (Tom Mattice) provided in kind logistical support. Mike Janes and Alan Gordon assisted with site selection and sample collection. Mo Michels and Kelly Gerlach assisted with sample preparation. Mac Wilson, Pat Dryer, John Seymour, and Richard Carstensen assisted with field work.

References

Abatzoglou, J. T. (2010). Influence of the PNA on declining mountain snowpack in the Western United States. *International Journal of Climatology*, *31*(8), 1135–1142. https://doi.org/10.1002/joc.2137

Armstrong, R. L., & Armstrong, B. (1987). Snow and avalanche climates of the western United States: A comparison of maritime, intermountain, and continental conditions. In *The Davos Symposium, September, 1986, avalanche formation, movement and effects* (Vol. 162, pp. 281–294). IAHS Publication.

Ballesteros-Canovas, J. A., Trappmann, D., Madrigal-Gonzalez, J., Eckert, N., & Stoffel, M. (2018). Climate warming enhances snow avalanche risk in the Western Himalayas. *Proceedings of the National Academy of Sciences*, *115*(13), 3410–3415. https://doi.org/10.1073/pnas.1716913115

Bartelt, P., Bühler, Y., Buser, O., Christen, M., & Meier, L. (2012). Modeling mass-dependent flow regime transitions to predict the stopping and depositional behavior of snow avalanches. *Journal of Geophysical Research*, *117*(F1), F01015. https://doi.org/10.1029/2010jf001957

Bebi, P., Kulakowski, D., & Rixen, C. (2009). Snow avalanche disturbances in forest ecosystems-State of research and implications for management. *Forest Ecology and Management*, *257*(9), 1883–1892. https://doi.org/10.1016/j.foreco.2009.01.050

Bellaire, S., Jamieson, B., Thumlert, S., Goodrich, J., & Statham, G. (2016). Analysis of long-term weather, snow and avalanche data at Glacier National Park, B.C., Canada. *Cold Regions Science and Technology*, *121*, 118–125. https://doi.org/10.1016/j.coldregions.2015.10.010

Birkeland, K. W., & Mock, C. J. (1996). Atmospheric circulation patterns associated with heavy snowfall events, Bridger Bowl, Montana, USA. *Mountain Research and Development*, *16*(3), 281–286. https://doi.org/10.2307/3673951

Birkeland, K. W., Mock, C. J., & Shinker, J. J. (2001). Avalanche extremes and atmospheric circulation patterns. *Annals of Glaciology*, *32*, 135–140. https://doi.org/10.3189/172756401781819030

Blöschl, G. (1999). Scaling issues in snow hydrology. *Hydrological Processes*, *13*(14–15), 2149–2175. https://doi.org/10.1002/(sici)1099-1085(199910)13:14/15<2149::aid-hyp847>3.0.co;2-8

Burrows, C. J., & Burrows, V. L. (1976). *Procedures for the study of snow avalanche chronology using growth layers of woody plants, occasional paper no. 23, report* (p. 56). Institute of Arctic and Alpine Research, Universtiy of Colorado.

Butler, D. R., & Sawyer, C. F. (2008). Dendrogeomorphology and high-magnitude snow avalanches: A review and case study. *Natural Hazards and Earth System Sciences*, *8*(2), 303–309. https://doi.org/10.5194/nhess-8-303-2008

Castebrunet, H., Eckert, N., & Giraud, G. (2012). Snow and weather climatic control on snow avalanche occurrence fluctuations over 50 yr in the French Alps. *Climate of the Past*, *8*(2), 855–875. https://doi.org/10.5194/cp-8-855-2012

Corona, C., Lopez Saez, J., Stoffel, M., Bonnefoy, M., Richard, D., Astrade, L., & Berger, F. (2012). How much of the real avalanche activity can be captured with tree rings? An evaluation of classic dendrogeomorphic approaches and comparison with historical archives. *Cold Regions Science and Technology*, *74–75*, 31–42. https://doi.org/10.1016/j.coldregions.2012.01.003

Dixon, R. W., Butler, D. R., Dechano, L. M., & Henry, J. A. (1999). Avalanche hazard in Glacier National Park: An El Nino connection? *Physical Geography*, *20*(6), 461–467. https://doi.org/10.1080/02723646.1999.10642690

Eckert, N., Keylock, C. J., Castebrunet, H., Lavigne, A., & Naaim, M. (2013). Temporal trends in avalanche activity in the French Alps and subregions: From occurrences and runout altitudes to unsteady return periods. *Journal of Glaciology*, *59*(213), 93–114. https://doi.org/10.3189/2013JoG12J091

Eckert, N., Parent, E., Kies, R., & Baya, H. (2009). A spatio-temporal modelling framework for assessing the fluctuations of avalanche occurrence resulting from climate change: Application to 60 years of data in the northern French Alps. *Climatic Change*, *101*(3–4), 515–553. https://doi.org/10.1007/s10584-009-9718-8

Eckert, N., Parent, E., Kies, R., & Baya, H. (2010). A spatio-temporal modelling framework for assessing the fluctuations of avalanche occurrence resulting from climate change: Application to 60 years of data in the northern French Alps. *Climatic Change*, *101*(3–4), 515–553. https://doi.org/10.1007/s10584-009-9718-8

Favillier, A., Guillet, S., Lopez-Saez, J., Giacona, F., Eckert, N., Zenhäusern, G., et al. (2023). Identifying and interpreting regional signals in tree-ring based reconstructions of snow avalanche activity in the Goms valley (Swiss Alps). *Quaternary Science Reviews*, *307*, 108063. https://doi.org/10.1016/j.quascirev.2023.108063

Favillier, A., Guillet, S., Morel, P., Corona, C., Lopez Saez, J., Eckert, N., et al. (2017). Disentangling the impacts of exogenous disturbances on forest stands to assess multi-centennial tree-ring reconstructions of avalanche activity in the upper Goms Valley (Canton of Valais, Switzerland). *Quaternary Geochronology*, *42*, 89–104. https://doi.org/10.1016/j.quageo.2017.09.001

Favillier, A., Guillet, S., Trappmann, D., Morel, P., Lopez-Saez, J., Eckert, N., et al. (2018). Spatio-temporal maps of past avalanche events derived from tree-ring analysis: A case study in the Zermatt valley (Valais, Switzerland). *Cold Regions Science and Technology*, *154*, 9–22. https://doi.org/10.1016/j.coldregions.2018.06.004

Fitzharris, B. B., & Bakkehoi, S. (1986). A synoptic climatology of major avalanche winters in Norway. *Journal of Climatology*, *6*(4), 431–446. https://doi.org/10.1002/joc.3370060408

Fitzharris, B. B., & Schaerer, P. A. (1980). Frequency of major avalanche winters. *Journal of Glaciology*, *26*(94), 43–52. https://doi.org/10.3189/s0022143000010571

Fleming, S. W., & Whitfield, P. H. (2010). Spatiotemporal mapping of ENSO and PDO surface meteorological signals in British Columbia, Yukon, and southeast Alaska. *Atmosphere-Ocean*, *48*(2), 122–131. https://doi.org/10.3137/ao1107.2010

Gauthier, F., Germain, D., & Hétu, B. (2017). Logistic models as a forecasting tool for snow avalanches in a cold maritime climate: Northern Gaspésie, Québec, Canada. *Natural Hazards*, *89*(1), 201–232. https://doi.org/10.1007/s11069-017-2959-3

Germain, D. (2016). A statistical framework for tree-ring reconstruction of high-magnitude mass Movements: Case study of snow avalanches in eastern Canada. *Geografiska Annaler - Series A: Physical Geography*, *98*(4), 303–311. https://doi.org/10.1111/geoa.12138

Germain, D., Filion, L., & Hétu, B. (2009). Snow avalanche regime and climatic conditions in the Chic-Choc Range, eastern Canada. *Climatic Change*, *92*(1–2), 141–167. https://doi.org/10.1007/s10584-008-9439-4

Germain, D., Hétu, B., & Filion, L. (2010). Tree-ring based reconstruction of past snow avalanche events and risk assessment in Northern Gaspé Peninsula (Québec, Canada). In M. Stoffel, M. Bollschweiler, D. R. Butler, & B. H. Luckman (Eds.), *Tree rings and natural hazards—A state-of-the-art*. Springer.

GHCN. (2022). Global historical Climatology network (GHCN). Retrieved from https://www.ncei.noaa.gov/products/land-based-station/global-historical-climatology-network-daily

Giacona, F., Eckert, N., Corona, C., Mainieri, R., Morin, S., Stoffel, M., et al. (2021). Upslope migration of snow avalanches in a warming climate. *Proceedings of the National Academy of Sciences*, *118*(44). https://doi.org/10.1073/pnas.2107306118

Google. (2023). Imagery of study area, using R statistical package GGMAP. Retrieved from https://cran.r-project.org/web/packages/ggmap/ggmap.pdf

Gratton, M., Germain, D., & Boucher, É. (2020). Meteorological triggering scenarios of tree-ring-based snow avalanche occurrence on scree slopes in a maritime climate, Eastern Canada. *Physical Geography*, *41*, 1–18. https://doi.org/10.1080/02723646.2019.1573622

Greene, E., Birkeland, K. W., Elder, K., McCammon, I., Staples, M., & Sharaf, D. (2016). *Snow, weather, and avalanches: Observation guidelines for avalanche programs in the United States* (3rd ed., p. 104). American Avalanche Association.

Haegeli, P., Shandro, B., & Mair, P. (2021). Using avalanche problems to examine the effect of large-scale atmosphere–ocean oscillations on avalanche hazard in western Canada. *The Cryosphere*, *15*(3), 1567–1586. https://doi.org/10.5194/tc-15-1567-2021

Hebertson, E. G., & Jenkins, M. J. (2003). Historic climate factors associated with major avalanche years on the Wasatch Plateau, Utah. *Cold Regions Science and Technology*, *37*(3), 315–332. https://doi.org/10.1016/S0165-232x(03)00073-9

Hennon, P. E., McClellan, M. H., & Palkovic, P. (2002). Comparing deterioration and ecosystem function of decay-resistant and decay-susceptible species of dead trees. In *USDA forest service general technical report, PSW-GTSR-181* (pp. 435–444).

ITRDB. (2020). International tree ring data bank (ITRDB). Retrieved from https://www.ncei.noaa.gov/products/paleoclimatology/tree-ring

Keylock, C. J. (2003). The North Atlantic oscillation and snow avalanching in Iceland. *Geophysical Research Letters*, *30*(5), 1254. https://doi.org/10.1029/2002gl016272

Kogelnig-Mayer, B., Stoffel, M., Schneuwly-Bollschweiler, M., Hübl, J., & Rudolf-Miklau, F. (2011). Possibilities and limitations of dendrogeomorphic time-series reconstructions on sites influenced by debris flows and frequent snow avalanche activity. *Arctic Antarctic and Alpine Research*, *43*(4), 649–658. https://doi.org/10.1657/1938-4246-43.4.649

Lader, R., Bidlack, A., Walsh, J. E., Bhatt, U. S., & Bieniek, P. A. (2020). Dynamical downscaling for southeast Alaska: Historical climate and future projections. *Journal of Applied Meteorology and Climatology*, *59*(10), 1607–1623. https://doi.org/10.1175/jamc-d-20-0076.1

Laternser, M., & Schneebeli, M. (2002). Temporal trend and spatial distribution of avalanche activity during the last 50 years in Switzerland. *Natural Hazards*, *27*(3), 201–230. https://doi.org/10.1023/a:1020327312719

Laternser, M., & Schneebeli, M. (2003). Long-term snow climate trends of the Swiss Alps (1931–99). *International Journal of Climatology*, *23*(7), 733–750. https://doi.org/10.1002/joc.912

Malevich, S. B., Guiterman, C. H., & Margolis, E. Q. (2018). burnr: Fire history analysis and graphics in R. *Dendrochronologia*, *49*, 9–15. https://doi.org/10.1016/j.dendro.2018.02.005

Margreth, S. (2011). *Avalanche mitigation study: Behrends avenue avalanche path and white Subdivision avalanche path, Juneau, Alaska, SLF expert report G2011.21*. WSL-Institut für Schnee- und Lawinenforschung SLF.

Marienthal, A., Hendrikx, J., Birkeland, K., & Irvine, K. M. (2015). Meteorological variables to aid forecasting deep slab avalanches on persistent weak layers. *Cold Regions Science and Technology*, *120*, 227–236. https://doi.org/10.1016/j.coldregions.2015.08.007

Martin, J. P., & Germain, D. (2016). Dendrogeomorphic reconstruction of snow avalanche regime and triggering weather conditions: A classification tree model approach. *Progress in Physical Geography*, *40*(4), 527–548. https://doi.org/10.1177/0309133315625863

Martin, J.-P., & Germain, D. (2017). Large-scale teleconnection patterns and synoptic climatology of major snow-avalanche winters in the Presidential Range (New Hampshire, USA). *International Journal of Climatology*, *37*, 109–123. https://doi.org/10.1002/joc.4985

McCabe, G. J. (1994). Relationships between atmospheric circulation and snowpack in the Gunnison river basin, Colorado. *Journal of Hydrology*, *157*(1–4), 157–175. https://doi.org/10.1016/0022-1694(94)90103-1

McCabe, G. J., & Dettinger, M. D. (2002). Primary modes and predictability of year-to-year snowpack variations in the Western United States from teleconnections with Pacific ocean climate. *Journal of Hydrometeorology*, *3*(1), 13–25. https://doi.org/10.1175/1525-7541(2002)003%3C0013:PMAPOY%3E2.0.CO;2

Mock, C. J. (1996). Climatic controls and spatial variations of precipitation in the western United States. *Journal of Climate*, *9*(5), 1111–1125. https://doi.org/10.1175/1520-0442(1996)009<1111:ccasvo>2.0.co;2

Mock, C. J., & Birkeland, K. W. (2000). Snow avalanche climatology of the western United States mountain ranges. *Bulletin of the American Meteorological Society*, *81*(10), 2367–2392. https://doi.org/10.1175/1520-0477(2000)081<2367:sacotw>2.3.co;2

Mock, C. J., Carter, K. C., & Birkeland, K. W. (2016). Some perspectives on avalanche climatology. *Annals of the Association of American Geographers*, *107*(2), 1–10. https://doi.org/10.1080/24694452.2016.1203285

Morin, S., Horton, S., Techel, F., Bavay, M., Coléou, C., Fierz, C., et al. (2019). Application of physical snowpack models in support of operational avalanche hazard forecasting: A status report on current implementations and prospects for the future. *Cold Regions Science and Technology*, *170*, 102910. https://doi.org/10.1016/j.coldregions.2019.102910

Mote, P. W., Li, S., Lettenmaier, D. P., Xiao, M., & Engel, R. (2018). Dramatic declines in snowpack in the western US. *npj Climate and Atmospheric Science*, *1*(1–5), 2. https://doi.org/10.1038/s41612-018-0012-1

Neal, E. G., Walter, M. T., & Coffeen, C. (2002). Linking the pacific decadal oscillation to seasonal stream discharge patterns in southeast Alaska. *Journal of Hydrology*, *263*(1–4), 188–197. https://doi.org/10.1016/s0022-1694(02)00058-6

NOAA. (2022). NOAA (National oceanic and atmospheric administration) NWS (National weather Service) monthly climate normals (1991–2020) for Juneau airport. Retrieved from https://www.weather.gov/arh/climate?wfo=ajk

Nowacki, G. J., & Abrams, M. D. (1997). Radial-growth averaging criteria for reconstruction disturbance histories from presettlement-origin oaks. *Ecological Monographs*, *67*(2), 225–249. https://doi.org/10.2307/2963514

Ott, R. L., & Longnecker, M. T. (2016). *An introduction to statistical methods and data analysis* (7th ed. ed.). Cengage Learning.

Papineau, J. M. (2001). Wintertime temperature anomalies in Alaska correlated with ENSO and PDO. *International Journal of Climatology*, *21*(13), 1577–1592. https://doi.org/10.1002/joc.686

Pederson, G. T., Betancourt, J. L., & McCabe, G. J. (2013). Regional patterns and proximal causes of the recent snowpack decline in the Rocky Mountains, U.S. *Geophysical Research Letters*, *40*(9), 1811–1816. https://doi.org/10.1002/grl.50424

Pederson, G. T., Gray, S. T., Ault, T., Marsh, W., Fagre, D. B., Bunn, A. G., et al. (2011a). Climatic controls on the snowmelt hydrology of the northern Rocky mountains. *Journal of Climate*, *24*(6), 1666–1687. https://doi.org/10.1175/2010JCLI3729.1

Pederson, G. T., Gray, S. T., Woodhouse, C. A., Betancourt, J. L., Fagre, D. B., Littell, J. S., et al. (2011b). The unusual nature of recent snowpack declines in the North American Cordillera. *Science*, *333*(6040), 332–335. https://doi.org/10.1126/science.1201570

Peitzsch, E. H., Hendrikx, J., Stahle, D. K., Pederson, G. T., Birkeland, K. W., & Fagre, D. B. (2021). A regional spatiotemporal analysis of large magnitude snow avalanches using tree rings. *Natural Hazards and Earth System Sciences*, *21*(2), 533–557. https://doi.org/10.5194/nhess-21-533-2021

Peitzsch, E. H., Pederson, G. T., Birkeland, K. W., Hendrikx, J., & Fagre, D. B. (2021). Climate drivers of large magnitude snow avalanche years in the U.S. northern Rocky Mountains. *Scientific Reports*, *11*(1), 10032. https://doi.org/10.1038/s41598-021-89547-z

Peitzsch, E. H., Stahle, D. K., Hood, E. W., Zeibig-Kichas, N., & Milone, K. M. (2023). *Tree ring dataset for a regional avalanche chronology in southeast Alaska, 1396–2019*. U.S. Geological Survey Data Release. https://doi.org/10.5066/P9LPZPJP

Pelto, M., Kavanaugh, J., & McNeil, C. (2013). Juneau icefield mass balance program 1946–2011. *Earth System Science Data*, *5*(2), 319–330. https://doi.org/10.5194/essd-5-319-2013

Pielmeier, C., Techel, F., Marty, C., & Stucki, T. (2013). Wet snow avalnache activity in the Swiss Alps—Trend analysis for mid-winter season. In F. Naaim-Bouvet, Y. Durand, & R. Lambert (Eds.), *Proceedings of the international snow science workshop, October 7–13, Grenoble, France* (pp. 1240–1246).

Pop, O. T., Munteanu, A., Flaviu, M., Gavrilă, I.-G., Timofte, C., & Holobâcă, I.-H. (2018). Tree-ring-based reconstruction of high-magnitude snow avalanches in piatra craiului mountains (southern carpathians, Romania). *Geografiska Annaler Series A: Physical Geography*, *100*(2), 99–115. https://doi.org/10.1080/04353676.2017.1405715

Reardon, B. A., Pederson, G. T., Caruso, C. J., & Fagre, D. B. (2008). Spatial reconstructions and comparisons of historic snow avalanche frequency and extent using tree rings in Glacier National Park, Montana, U.S.A. *Arctic Antarctic and Alpine Research*, *40*(1), 148–160. https://doi.org/10.1657/1523-0430(06-069)[reardon]2.0.co;2

Reuter, B., van Herwijnen, A., Veitinger, J., & Schweizer, J. (2015). Relating simple drivers to snow instability. *Cold Regions Science and Technology*, *120*, 168–178. https://doi.org/10.1016/j.coldregions.2015.06.016

Rixen, C., Haag, S., Kulakowski, D., & Bebi, P. (2007). Natural avalanche disturbance shapes plant diversity and species composition in subalpine forest belt. *Journal of Vegetation Science*, *18*(5), 735–A737. https://doi.org/10.1111/j.1654-1103.2007.tb02588.x

Shandro, B., & Haegeli, P. (2018). Characterizing the nature and variability of avalanche hazard in western Canada. In *Natural hazards and Earth system sciences discussions* (pp. 1–32). https://doi.org/10.5194/nhess-2018-2

Shanley, C. S., Pyare, S., Goldstein, M. I., Alaback, P. B., Albert, D. M., Beier, C. M., et al. (2015). Climate change implications in the northern coastal temperate rainforest of North America. *Climatic Change*, *130*(2), 155–170. https://doi.org/10.1007/s10584-015-1355-9

Shroder, J. F. (1978). Dendrogeomorphological analysis of mass movement on Table Cliffs Plateau, Utah. *Quaternary Research*, *9*(2), 168–185. https://doi.org/10.1016/0033-5894(78)90065-0

Stoffel, M., Bollschweiler, M., Butler, D. R., & Luckman, B. H. (Eds.). (2010). *Tree rings and natural hazards—A state of the art* (p. 505). Springer Science and Business Media.

Thompson, D. W. J., & Wallace, J. M. (1998). The Arctic oscillation signature in the wintertime geopotential height and temperature fields. *Geophysical Research Letters*, *25*(9), 1297–1300. https://doi.org/10.1029/98gl00950

Thompson, D. W. J., & Wallace, J. M. (2000). Annular modes in the extratropical circulation. Part I: Month-to-month variability. *Journal of Climate*, *13*(5), 1000–1016. https://doi.org/10.1175/1520-0442(2000)013<1000:amitec>2.0.co;2

Webb, E. J., & Magi, B. I. (2022). The Ensemble Oceanic Niño Index. *International Journal of Climatology*, *42*(10), 5321–5341. https://doi.org/10.1002/joc.7535

Wilbur, C., Mears, A. I., LaRue, D., & Glude, B. (2010). A light-weight splitting wedge to protect Tower 4/6 Snettisham Transmission Line, Southeast Alaska. In *Proceedings of the international snow science workshop, squaw valley, CA, USA, October 17–27, 2010*.